Salt-Compact Albumin as a New Pure Protein-based Biomaterials: From Design to In Vivo Studies

Eya Aloui, Jordan Beurton, Claire Medemblik, Ludivine Hugoni, Igor Clarot, Ariane Boudier, Youri Arntz, Marcella de Giorgi, Jérôme Combet, Guillaume Fleith, et al.

ADVANCED HEALTHCARE MATERIALS
www.advhealthmat.de

Salt-Compact Albumin as a New Pure Protein-based Biomaterials: From Design to In Vivo Studies

Eya Aloui, Jordan Beurton, Claire Medemblik, Ludivine Hugoni, Igor Clarot, Ariane Boudier, Youri Arntz, Marcella De Giorgi, Jérôme Combet, Guillaume Fleith, Eric Mathieu, Naji Kharouf, Leyla Kocgozlu, Benoît Heinrich, Damien Favier, Michael Brender, Fouzia Boulmedais, Pierre Schaaf, Benoît Frisch, and Philippe Lavalle**

Current biodegradable materials are facing many challenges when used for the design of implantable devices because of shortcomings such as toxicity of crosslinking agents and degradation derivatives, limited cell adhesion, and limited immunological compatibility. Here, a class of materials built entirely of stable protein is designed using a simple protocol based on salt-assisted compaction of albumin, breaking with current crosslinking strategies. Salt-assisted compaction is based on the assembly of albumin in the presence of high concentrations of specific salts such as sodium bromide. This process leads, surprisingly, to water-insoluble handable materials with high preservation of their native protein structures and Young's modulus close to that of cartilage (0.86 MPa). Furthermore, these materials are non-cytotoxic, non-inflammatory, and in vivo implantations (using models of mice and rabbits) demonstrate a very slow degradation rate of the material with excellent biocompatibility and absence of systemic inflammation and implant failure. Therefore, these materials constitute promising candidates for the design of biodegradable scaffolds and drug delivery systems as an alternative to conventional synthetic degradable polyester materials.

1. Introduction

The study of the interaction between oppositely charged polymers dates back to the 1930th when Bungenberg de Jong and Kruyt showed that by mixing a polyanion and a polycation a highly viscous fluid phase named coacervate is obtained.[1] In the 1990th, Decher et al., introduced polyelectrolyte multilayers obtained by the alternate deposition of polyanions and polycations onto a substrate, forming films that can reach several micrometers in thickness.[2] In 2009, Schlenoff et al., showed that polyelectrolyte complexes can be compacted and extruded in the presence of high salt concentrations to form processable materials[3–5] and in 2015, Mano et al., introduced a new way to get these materials by water evaporation from solutions of polyelectrolyte complexes prepared with high salt concentrations.[6,7]

E. Aloui, J. Beurton, C. Medemblik, L. Hugoni, Y. Arntz, M. De Giorgi, E. Mathieu, N. Kharouf, L. Kocgozlu, P. Schaaf, B. Frisch, P. Lavalle
Inserm UMR_S 1121, CNRS EMR 7003
Université Strasbourg, Biomaterials and Bioengineering
Centre de Recherche en Biomédecine de Strasbourg
Strasbourg F-67000, France
E-mail: frisch@unistra.fr; philippe.lavalle@inserm.fr

J. Beurton, I. Clarot, A. Boudier
Université de Lorraine
CITHEFOR
Nancy F-54000, France

J. Beurton, I. Clarot, A. Boudier
Université de Lorraine, CNRS
LRGP
Nancy F-54000, France

A. Boudier
Institut Universitaire de France (IUF)
Paris, France

J. Combet, G. Fleith, M. Brender, F. Boulmedais, P. Schaaf
Université de Strasbourg, CNRS
Institut Charles Sadron UPR22
Strasbourg F-67034, France

B. Heinrich, D. Favier
Université de Strasbourg, CNRS
Institut de Physique et Chimie des Matériaux de Strasbourg UMR 7504
Strasbourg F-67034, France

The ORCID identification number(s) for the author(s) of this article can be found under https://doi.org/10.1002/adhm.202403385

DOI: 10.1002/adhm.202403385

The electrostatic interactions between the charged moieties of the polyanions and the polycations and their competition with salt ions are responsible for the formation of these materials, currently known as Compact Polyelectrolyte Complexes (CoPECs).[3–7] CoPECs were obtained using synthetic polyelectrolytes as well as natural polysaccharides such as alginate and chitosan.[6,8,9]

Interestingly, proteins are macromolecules that usually possess both positive and negative patches. To go even further with "biological" materials, in a first attempt to form materials with a protein, we mixed albumin with a natural polyelectrolyte (chitosan) in the presence of salt. Surprisingly, by decreasing chitosan concentration down to zero, we discovered that albumin in the presence of specific salts can form a material on its own without any "partner" like chitosan. This new material made entirely from a protein, bovine serum albumin (BSA), without using any crosslinking agent, is reported here. Such material, to our knowledge, has never been described previously. The formulation of the material follows the same strategy as that for CoPECs obtained by evaporation of solutions of polyelectrolyte complexes in the presence of high salt concentrations.[6] We selected albumin primarily because of its biocompatibility and biodegradability.[10] Furthermore, albumin, the most abundant protein in plasma, is a versatile carrier for many drugs and substances and it can be produced at low cost and easily functionalized.[10–12]

Due to their biocompatibility, biodegradability, bioactivity, low immunogenicity, relatively low cost, and the possibility of autologous material production, albumin-based biomaterials are attracting and show an increasing interest in various biomedical applications such as tissue engineering, coating of implantable devices, and drug release.[10,13–15] Albumin-based materials were already fabricated using a large number of processing techniques such as freeze-drying, solution evaporation, electrospinning, and 3D printing.[10,14–17] These materials are usually produced by heat aggregation, pH-induced gelation, or chemical crosslinking.[10,14,15,18–23] However, all methods described in previous studies require the addition of a crosslinking step of the proteins, which can be attained by using chemical agents such as glutaraldehyde or formaldehyde, enzymes such as transglutaminase, or heat aggregation at high temperature and alkaline pH.[10,14,15,18–23] The use of high temperatures, extreme pH levels, and cross-linking agents leads most of the time to irreversible denaturation. This can result in a loss of its original biological properties with the risk of generating new antigenic sites which could trigger a strong inflammatory response.[10,12,24]

In the present work, we propose a full study of this new class of biomaterials where we investigate the formation of albumin materials by evaporation under non-denaturing experimental conditions (37 °C and pH 6) in the presence of salts. The prepared albumin materials were then characterized and we evaluated for their biocompatibility and biodegradability in vitro and in vivo.

2. Experimental Section

2.1. Chemical Reagents

From Acros Organics were purchased Bovine Serum Albumin (BSA, fraction V, ≥ 96%) and potassium bromide (KBr). Human Serum Albumin (HSA, ≥ 96%) was purchased from SeraCare. From Sigma–Aldrich were purchased recombinant Human Serum Albumin (rHSA, produced in rice, ≥ 96%), ovalbumin (OVA, ≥ 98%), Rabbit Serum Albumin (RbSA, ≥ 99%), Rat Serum Albumin (RtSA, ≥ 96%), Porcine Serum Albumin (PSA, ≥ 96%), γ-globulins from human blood (≥ 99%), sodium bromide (NaBr), calcium chloride dihydrate ($CaCl_2$, $2H_2O$), potassium chloride (KCl), potassium acetate (AcOK), and D_2O. Sodium chloride (NaCl) was purchased from VWR Chemicals. Sodium iodide (NaI) and dipotassium phosphate (K_2HPO_4) were obtained from Prolabo. Potassium iodide (KI) was purchased from Carbo Erba Reagents. Magnesium chloride ($MgCl_2$, anhydrous) and ammonium formate (NH_4HCO_2) were purchased from Fluka. Potassium carbonate (K_2CO_3) was purchased from Alfa Aesar.

2.2. Cell Culture

BALB/c 3T3 mouse fibroblasts (clone A31 ATCC CCL-163) were cultivated in Dulbecco's Modified Eagle Medium High Glucose (DMEM) containing stabilized glutamine and sodium pyruvate (Dutscher), supplemented with 10% (v/v) of fetal bovine serum (FBS, Dutscher) and 1% (v/v) of Penicillin-Streptomycin Solution 100X (PS, final concentrations: 0.06 mg mL^{-1} and 0.1 mg mL^{-1} respectively) (Dutscher) at 37 °C in 5% CO_2, 95% humidity. Cells were harvested using trypsin (0.5 g L^{-1})-EDTA (0.2 g L^{-1}) (Dutscher) for 5 min at 37 °C. Thiazolyl Blue Tetrazolium Bromide (MTT) was purchased from Sigma–Aldrich. CellTiter Glo Viability Assay was purchased from Promega.

RAW 264.7 mouse macrophages (ATCC TIB-71) were cultivated inDMEM containing stabilized glutamine (Sigma–Aldrich), supplemented with 5% (v/v) of heat-inactivated fetal bovine serum (Gibco), penicillin (100 U mL^{-1}) (Sigma–Aldrich) and streptomycin (0.1 mg mL^{-1}) (Sigma–Aldrich) at 37 °C in 5% CO_2, 95% humidity. Cells were harvested using trypsin (0.5 g L^{-1})-EDTA (0.2 g L^{-1}) (Sigma–Aldrich) for 5 min at 37 °C. Lipopolysaccharide (LPS) from *Escherichia coli* (K12) was purchased from Invivogen. Purified anti-mouse Tumor Necrosis Factor-α (TNF-α) antibody clone 1F3F3D4 and biotinylated anti-mouse TNF-α antibody clone XT3/XT22 for ELISA testing were purchased from eBioscience/ThermoFisher Scientific. Horseradish Peroxidase Avidin (Avidin HRP) was purchased from Jackson. P-aminobenzenesulfonamide and acetic acid were purchased from Sigma–Aldrich. *N*-(1-naphtyl)ethylenediamine dihydrochloride was purchased from Acros Organics.

2.3. Formulation (General Procedure)

A solution of BSA (100 mg mL^{-1}) and NaBr (1 M) in an acetate buffer (0.2 M) at pH 6 was prepared. This solution was deposited in a non-stick silicone mold and evaporated at 37 °C for 7 days (for each membrane: mass of BSA deposited in the mold ≈800 mg, surface of the mold ≈7 cm^2). Next, the dry material was washed in milliQ water at room temperature for 48 h. The water-insoluble membrane was then collected and characterized. The molar ratio of salt/albumin was calculated using Equation (1).

$$Molar\ ratio\ salt/albumin = \frac{Molar\ concentration\ (salt)}{Molar\ concentration\ (albumin)} \quad (1)$$

The relative yield of the formulation was calculated using Equation (2). The density (Equation 3) of the material was assessed by immersion of the material in milliQ water (room temperature).

$$Relative\ yield\ (Y\%) = \frac{W_d}{W_{BSA}} \times 100 \quad (2)$$

$$Density = \frac{W_d}{V_d} \quad (3)$$

W_d represents the mass of the final dried membrane after washing in milliQ water for 48 h and drying in an oven at 37 °C overnight. V_d is the

volume of the dried membrane measured by immersion of the material in milliQ water (room temperature).

2.4. Stability in Aqueous Solutions

BSA/NaBr membranes were placed in 25 mL of the following dissolution media: milliQ water, physiological saline solution (0.9% NaCl), acidic medium (pH 3), alkaline medium (pH 10), saline solutions (1 M NaCl, 1 M NaBr), ethanol and a trypsin solution (0.5 g L^{-1}). Next, the media containing the membranes were incubated at 37 °C under stirring for 7 days. Then, the membranes were washed in milliQ water and dried at 37 °C for 24 h. The mass loss was calculated using Equation (4).

$$Mass\ loss\ (ML\%) = \frac{Initial\ mass\ (dry) - Final\ mass\ (dry)}{Initial\ mass\ (dry)} \times 100 \quad (4)$$

2.5. Salt Quantification by Inductively Coupled Plasma Optical Emission Spectroscopy

Quantification of sodium was carried out using an Inductively Coupled Plasma Optical Emission Spectroscopy (ICP-OES) method. Briefly, the material was mineralized in contact with 1.0 mL of H_2O and 3.0 mL of nitric acid 65%. The samples were then digested using a Microwave Digestion System (Multiwave GO, Anton Paar) for 50 min at 210 °C. The solution was recovered, and the volume was adjusted to 10.0 mL with 1% nitric acid aqueous solution. In parallel, a calibration curve of Na^+ from 0.01 to 1.00 mg L^{-1} in 1% nitric acid was realized. The solutions were injected using a peristaltic pump (set at 45 rpm) in the ICP system (ICP-OES, iCAP Pro, ThermoScientific) with argon as auxiliary gas. The nebulizing pressure was 2.1 bar and the flow rates of the nebulizer and cooler were 0.5 and 12.5 L min^{-1} respectively. Data acquisition was performed using Qtera software at the working wavelength of 588.995 nm.

2.6. Scanning Electron Microscopy (SEM) with Microanalysis and Atomic Force Microscopy (AFM)

SEM and microanalysis assessments were performed using a Quanta 250 FEG SEM (FEI Company, Eindhoven, The Netherlands) operating with an accelerated voltage of electrons of 10 kV. For SEM experiments, BSA/NaBr membranes were dried and then coated with a gold-palladium alloy using a Hummer Jr sputtering device (Technics, Union City, CA, USA). Electron-excited X-ray microanalysis was performed on randomly selected areas of the BSA/NaBr membranes with an accelerated voltage of electrons of 10 kV (emergence angle = 35 °, acquisition time = 100 s, process time = 7.68 µs). The amount of NaBr was estimated using the atomic percentage of bromine in the samples (%wt., analyzed surface = 2.8×10^6 μm^2, sample thickness = 1 mm). AFM investigations were carried out using a commercial microscope (BioScope Catalyst, Bruker USA). Images were acquired by tapping mode in liquid phase (water) using a ScanAsist-fluid cantilever with a spring constant of 0.7N m^{-1} and a resonance frequency in liquid of 50 kHz (Veeco probe, Bruker USA). The resolution of images was 512 × 512 (scan rate of 0.5 Hz). Image analysis was conducted with the Gwyddion shareware (Czech Metrology Institut, Czech Republik).

2.7. Tensile Testing

The tensile testing was performed using an Instron ElectroPulsTM E3000 equipped with a 100 N force sensor. A batch of six hydrated (in milliQ water) BSA/NaBr membranes was used. The samples were cut with a punch to form six specimens with standardized dimensions (initial useful length L_0 = 40 mm, effective initial width l_0 = 10 mm, initial thickness e_0 = 1.74 ± 0.079 mm). The tensile test was then performed at room temperature with a tensile speed of 0.1 mm s^{-1}. The elastic modulus (E) was calculated within the elastic domain of the strain (ϵ)-stress (σ) curve (Equation 5).

$$\sigma = E \times \varepsilon \quad (5)$$

2.8. Rheological Evaluation

The viscoelastic behavior of BSA/NaBr membranes (thickness ≈1.7 mm) was assessed using a rheometer Kinexus ultra + (Malvern, United Kingdom) in parallel plate configuration (20 mm diameter). Membranes were previously hydrated in milliQ water for 24 h. The BSA/NaBr discs were loaded between the plates, and the gap was closed until the sample was in good contact with both plates (normal force < 1 N). At the beginning of the experiment as well as between experiments, the samples were equilibrated for 5 min. During this time, the normal force decreased to values below 0.1 N in all samples. Amplitude sweep tests were conducted at shear strains ranging from 0.01% to 100% at a fixed frequency of 0.5 Hz and 25 °C. The shear modulus $G^*(\omega) = \sigma(\omega) / \gamma(\omega)$ follows from the ratio between stress (σ) and strain amplitude (γ). $G^*(\omega)$ = G' + iG" is a complex quantity with an elastic storage modulus (G') and viscous loss modulus (G"). The absolute magnitude of the shear modulus, |G*|, was calculated using Equation (6).

$$|G^*| = \left(G'^2 + G''^2\right)^{0.5} \quad (6)$$

For relaxation time tests, a shear strain of 1% was applied on the membranes for 15 min at 25 °C. The curve shear stress = f(time(s)) was used to evaluate the relaxation of the tested materials throughout the experiments. The time at which the measured shear stress was reduced by half (Rt(1/2)) was determined.

2.9. In Vitro Biological Evaluation

The membranes used for in vitro biological evaluation (BSA/NaBr) were washed in ethanol 70% then with sterile Phosphate Buffered Saline (PBS) 1X and sterilized for 15 min under UV light. Extract cytotoxicity and direct cytotoxicity tests were performed according to the ISO standard 10993–5 (2009). The normalized metabolic activity was used to determine the percentage of viable cells in each group.

2.9.1. Extract Cytotoxicity Test

Each membrane sample (≈100 mg) was transferred to a 12-well plate and extracted in 1.5 mL of culture medium (DMEM + FBS (10%) + PS (1%)) under stirring at 37 °C for 72 h. Dilutions containing 12.5%, 25%, 50%, and 100% (v/v) of the extracts were then prepared. BALB/c 3T3 fibroblasts were cultivated in a 96-well plate at 8×10^3 cells per well (DMEM + FBS (10%) + PS (1%)) at 37 °C for 24 h. Then, the culture medium in each well was replaced with 100 µL of the extract dilutions. Positive and negative controls were prepared with fresh culture media and with dimethyl sulfoxide (DMSO) diluted in culture media (20% v/v) respectively. The plate was incubated at 37 °C for 24 h. After incubation, the culture medium in each well was replaced with 100 µL of a solution of MTT (1 mg mL^{-1}, diluted in culture medium), and the plate was incubated at 37 °C for 2 h. The MTT solution was replaced with 80 µL of DMSO. The absorbance at 560 nm was measured using a spectrophotometer (SAFAS, Monaco).

2.9.2. Direct Cytotoxicity Test

BSA/NaBr membranes (diameter = 5 mm, thickness = 0.7 mm) were transferred to a black-walled 96-well plate. BALB/c 3T3 fibroblasts were

added to the plate at 8×10^3 cells per well (DMEM + FBS (10%) + PS (1%)). Positive and negative controls were added with fresh culture media and with DMSO diluted in culture media (20% v/v) respectively. The plate was incubated at 37 °C for 24 h. After incubation, the culture medium in each well was replaced with 100 µL of CellTiter-Glo reagent (diluted in culture media, 50% v/v). The bioluminescence was measured using a spectrophotometer (SAFAS, Monaco).

2.9.3. Macrophage Activation Assay

BSA/NaBr membranes (diameter = 5 mm, thickness = 0.7 mm) were transferred to a 96-well plate. RAW 264.7 macrophages were added to the plate at 10^5 cells per well (DMEM + FBS (5%) + PS (1%)). After 24 h of incubation at 37 °C, LPS was added to the LPS-treated groups to obtain a final concentration of 50 ng mL^{-1} in each well. The plate was then incubated for another 24 h at 37 °C. Untreated and LPS-treated controls were prepared with fresh culture media and with culture media containing 50 ng mL^{-1} of LPS respectively. The supernatants were collected for NO and TNF-α production assessments.

Concentrations of nitrite in cell supernatants were evaluated by the Griess test. 60 µL of Griess reagent (v/v mixture of 58.1 mM *p*-aminobenzene sulfonamide in 30% acetic acid and 3.9 mM *N*-(1-naphtyl)ethylenediamine dihydrochloride in 60% acetic acid) was added to 40 µL of supernatant and the absorbance at 543 nm was measured using a spectrophotometer (SAFAS, Monaco).

TNF-α concentration in cell supernatants was evaluated by ELISA using commercially available reagents and following the manufacturer's instructions. Samples were diluted with culture media (DMEM + FBS (5%) + PS (1%)) and incubated with capture antibody (2 h, 37 °C). Detection antibody (0.5 µg mL^{-1} in PBS, 0.05% Tween 20, and 1% BSA) was added for 1 h at 37 °C). Avidin HRP was then introduced (45 min, 37 °C). A solution of tetramethylbenzidine (1.25 mM) and H_2O_2 (13.05 mM) in 0.1 M pH 5 citrate buffer was added. After the addition of HCl (1 M), the absorbance at 450 nm was measured using a spectrophotometer (SAFAS, Monaco).

2.10. In Vivo Biocompatibility Evaluation

For in vivo evaluation, albumin materials were prepared in the shape of cylinders for subcutaneous implantation in the tested animals. The following solutions were prepared: BSA/NaBr (BSA and NaBr concentrations of 200 mg mL^{-1} and 1.2 M respectively), BSA/$CaCl_2$ (BSA and $CaCl_2$ concentrations of 200 mg mL^{-1} and 2.1 M respectively), HSA/NaBr (HSA and NaBr concentrations of 200 mg mL^{-1} and 1.2 M respectively), HSA/$CaCl_2$ (HSA and $CaCl_2$ concentrations of 200 mg mL^{-1} and 2.1 M respectively), and RbSA/AcOK (RbSA and AcOK concentrations of 200 mg mL^{-1} and 4.8 M respectively). The solutions were placed into cylindrical molds and evaporated for 21 days. Then, the materials were washed in milliQ water, cut to fit the size recommendation for subcutaneous implants, and dried at 37 °C for 24 h. The dry batches of implants were transferred to a sub-contractor (Aerial, France) for sterilization using electron beam irradiation (25 kGy). Before subcutaneous implantation, the implants were rehydrated in PBS 1X under sterile conditions for 18 h. Animal experiments were performed according to the ethical guidelines of animal experimentation.

2.10.1. Biocompatibility and Biodegradability Evaluation in Nude Mice

The following implants (dry and sterile) were transferred to a sub-contractor (PCBIS, France): BSA/NaBr (length ≈1 cm, diameter ≈3 mm, mass ≈80 mg), BSA/$CaCl_2$ (length ≈1 cm, diameter ≈2 mm, mass ≈40 mg), HSA/NaBr (length ≈1 cm, diameter ≈3 mm, mass ≈80 mg) and HSA/$CaCl_2$ (length ≈1 cm, diameter ≈2 mm, mass ≈40 mg). The experiment involved twelve healthy female NMRI-Nude mice (NMRI/Nu). Animals were 12 weeks old at the beginning of the treatment and were divided into four groups: group 1 (implanted with BSA/$CaCl_2$ materials, n = 3), group 2 (implanted with BSA/NaBr materials, n = 3), group 3 (implanted with HSA/$CaCl_2$ materials, n = 3), and group 4 (implanted with HSA/NaBr materials, n = 3). At D0, the animals were anesthetized with ketamine (75 mg kg^{-1}) and xylazine (5 mg kg^{-1}) before receiving implants (hydrated in PBS 1X) by subcutaneous route (D0), after an incision of 6 mm. Mice were sacrificed after 28 days (D28). Monitoring of clinical signs, local tolerance, and body weight was conducted twice a week from D0 until sacrifice. The size of the implants was measured using a caliper. After sacrifice, the implants and their surrounding tissues were harvested, fixed in formaldehyde, and embedded in paraffin (tissue processor Pearl, Leica Biosystems, Germany). They were then cut using a microtome (6 µm) and stained (trichrome Gömöri and Picro–Sirius stains). Gömöri trichrome staining highlighted cell bodies (blue–violet) and collagen (green), while Picro–Sirius staining was specific for collagen (red). All the usual precautions were taken during and after the surgery to ensure the well-being of the animals according to the APAFIS procedure n°2020022715005379 validated by the ethics committee of Strasbourg, the CREMEAS, and the Ministry of Education and Research.

2.10.2. Biocompatibility and Biodegradability Evaluation in NZW Rabbits

The following implants (dry and sterile) were transferred to a sub-contractor (C-Ris, France): RbSA/AcOK (length ≈1 cm, diameter ≈5 mm, mass ≈80 mg) and HSA/$CaCl_2$ (length ≈1 cm, diameter ≈4 mm, mass ≈80 mg). 15 healthy male New Zealand White (NZW) albino rabbits were obtained from Charles River Laboratory (France). The animals were 13 weeks old at the beginning of the treatment. Before treatment, rabbits were randomized according to body weight criteria in three groups: group 1 (control, n = 3), group 2 (implanted with RbSA/AcOK materials, n = 6), and group 3 (implanted with HSA/$CaCl_2$ materials, n = 6). At D0, the animals received buprenorphine analgesic (Buprecare) at 40 µg kg^{-1} (subcutaneously) 30 min before the anesthesia. Then, they were anesthetized with 2–5% isoflurane (2–5 L min^{-1}) and received lidocaine analgesic (Lurocaïne) at 0.3 mg kg^{-1} (infiltration route). Rabbits from HSA/$CaCl_2$ and RbSA/AcOK groups received implants (hydrated in PBS 1X) by a subcutaneous route at the interscapular region, after an incision of 1 cm. The control group received only an incision of 1 cm. Rabbits were sacrificed after 28 days (D28). Animals were anesthetized under isoflurane and exsanguinated by intracardiac puncture. Rabbits were then euthanized by a lethal intracardiac injection of Dolethal (1 mL kg^{-1}) and carotid arteries were cut for final exsanguination. Monitoring of clinical signs, local tolerance, and body weight was conducted twice a week from D0 until sacrifice. The size of the implants was measured using a caliper. Animals were fasted overnight before blood collection. At D0, D2, D14, and D28, blood was collected. Serum samples were used to quantify aspartate aminotransferase (ASAT) and alanine aminotransferase (ALAT), as well as inflammatory markers (C-Reactive Protein (CRP), Interleukin-6 (IL-6), IL-10, TNF-α, Interferon-γ (IFN-γ). ALAT and ASAT were quantified using the KBIO4-DUO biochemistry analyzer (Kitvia, France) according to the standard operating procedure. Inflammatory markers were quantified using ELISA kits.

2.11. Statistical Analysis

Data were analyzed by using R (version 3.6.1, R Foundation for Statistical Computing, Vienna, Austria). The normality of distribution was determined with the Shapiro–Wilk test. The equality of variances was determined with the F-test. When the data were normally distributed and the variances of the samples were equal, a *t*-test (2-tailed) was used to compare the two means. When these two conditions did not apply, a Mann–Whitney test was performed instead. Values were considered statistically significant at $p < 0.05$.

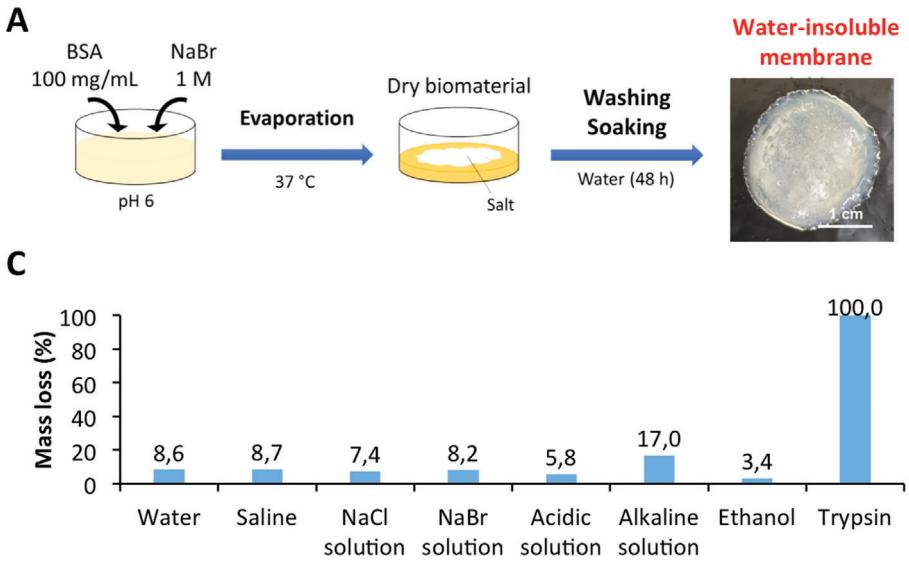

Salt	0.5 M	1 M	2 M
KCl	S	S	S
NaCl	S	S	S
KBr	S	S	S
NaBr	M	M	M
KI	M	M	F
NaI	M	F	F
$CaCl_2$	M	M	F
$MgCl_2$	S	M	M
$KC_2H_3O_2$	S	M	M
NH_4HCO_2	S	M	M
K_2CO_3	S	S	S
K_2HPO_4	S	S	S

Figure 1. Preparation of albumin materials by salt-assisted compaction. A) Formulation procedure. The evaporation is carried on in an oven (37 °C) for 7 days until the biomaterial is completely dry. After evaporation, washing, and soaking steps are applied to remove the salt, leaving a water-insoluble albumin material. B) The listed BSA/salt solutions were screened to identify the formulations leading to the formation of water-insoluble materials. Each solution (BSA concentration = 100 mg mL^{-1}, pH = 6) was evaporated for 7 days until the formation of a dry solid. The obtained solid was washed in milliQ water for 48 h. Only the formulation "M" produced water-insoluble and handable membranes. The formulation "S" produced water-soluble residues. The formulation "F" produced fragmented materials that were fragile and not handable. C) Stability of BSA/NaBr membranes in aqueous media, ethanol, and a solution of trypsin. For each dissolution media, three membranes were placed in 25 mL of media. The experiments were performed at 37 °C and under stirring for 7 days. Physiological saline solution (0.9% NaCl), NaCl solution (1 M), NaBr solution (1 M), acidic solution (pH = 3), alkaline solution (pH = 10), trypsin (0.5 mg mL^{-1}).

3. Results and Discussion

3.1. Salt-Compacted Albumin, an Unexpected Discovery

As part of our work on CoPECs[5,25,26] and natural polyelectrolytes,[8,9,27,28] we tested albumin for the preparation of naturally derived materials. At pH > pHi, albumin has a net negative charge and forms complexes with polycations.[29,30] Thus, we first prepared complexes usingBSA (pHi ≈4.7)[12] and chitosan at pH 6. Then, we evaporated the solution of BSA and chitosan in the presence of salt at 37 °C. This process was inspired by the work of Costa et al.,[6] and was selected to preserve the native structure of albumin.[18,31–33] After washing these materials in milliQ water for 48 h, we observed that only the materials prepared with low chitosan contents (<10% wt.) were water-insoluble. Therefore, we decided to test the possibility of eliminating the chitosan and evaluate the formation of these materials. The feasibility tests of this formulation were carried out by evaporation of a solution of BSA (100 mg mL^{-1}) in the presence of NaBr salt ranging from 0.5 to 2 M at pH 6 (**Figure 1A**). Unexpectedly, after washing with water (by soaking for 48 h), the obtained material (BSA/NaBr membrane) proved to be water-insoluble and exhibited good handability as a synthetic plastic material (Figure 1A).

In order to understand the composition of this water-insoluble protein material, we investigated the residual salt content of these materials after washing. The residual salt content in the washed BSA/NaBr materials was assessed using microanalysis on multiple samples of dried membranes prepared with NaBr concentrations ranging from 0.5 to 2 M. After evaporation of the solutions, the membranes were washed in milliQ water as described above and dried at 37 °C for 24 h. Electron-excited X-ray microanalysis performed on washed materials showed no signal at the specific energy of Bromine (1.480 KeV) indicating that the element Br was absent from all tested samples (Figure S1, Supporting Information). Furthermore, the analysis of these BSA/NaBr membranes. (green dots annotated (e)) by X-ray scattering revealed the absence of Bragg reflection signals (diffraction signal of X-rays by a crystalline structure, orange dots annotated (d)) meaning there is no crystalline NaBr in the membranes (Figure S14, Supporting Information). In order to complete the analysis of material composition after washing, residual sodium ions were quantified by ICP-OES. The mass percentage of sodium remaining in the material after washing was 0.09 (% m_{Na} / m_{BSA}), corresponding to less than 3 Na^+ ions per albumin. Br^- ions were not quantified by this method because their specific emission wavelength (154 nm) is outside the range (167–852 nm) of the detector used. In conclusion, these analyses show that Sodium and Bromine ions are absent or present in trace amounts in the materials after washing. These ions therefore do not contribute to material stability.

We showed that the NaBr used initially was eliminated during the washing process, leaving a stable material entirely made of water-insoluble albumin. We also verified that without salt, albumin did not assemble into water-insoluble materials in the tested conditions. Although the salting-out of protein was widely investigated,[34–38] the forming of organized and stable 3D networks from the salted-out protein was not previously reported, especially on such large scales. The formation of this material was surprising and never described before. Therefore, we directed our focus on studying this new class of albumin-based materials

by elucidating the key parameters for the formulation and by investigating their physicochemical and biological properties.

3.2. Salt is a Key Component for the Assembly of Albumin Materials

We investigated the Hoffmeister series[39] of salts to evaluate the effect of different salts on the formation of these materials. Screening of different salts (KCl, NaCl, KBr, NaBr, KI, NaI, $CaCl_2$, $MgCl_2$, AcOK, NH_4HCO_2, K_2CO_3, and K_2HPO_4) was performed at three different concentrations for each salt (0.5, 1, and 2 M).

This screening revealed that the preparation of albumin materials by salt-assisted compaction relied heavily on the type of salt used. Water-insoluble membranes were obtained with the following salts: NaBr, KI, NaI, $CaCl_2$, $MgCl_2$, AcOK, and NH_4HCO_2 (Figure 1B). The physical aspect and the properties of these membranes (water uptake, mechanical properties) varied depending on the type of salt used and its concentration, indicating that these two parameters are important for tuning the material's final properties (Figure S3, Supporting Information). For BSA solutions prepared with KCl, NaCl, or KBr, none of the tested concentrations led to the formation of water-insoluble materials. Water-soluble residues consisting of salt crystals surrounded by albumin deposits were obtained (Figure S2, Supporting Information). For the BSA solution prepared with K_2CO_3 and K_2HPO_4, albumin precipitation in the solution prior to its evaporation prevented membrane formation.

According to the Hoffmeister series, ions present in the solution exhibit different lyotropic effects on protein stability and solubility.[34–38] These effects were certainly involved in the formation of albumin materials by salt-assisted compaction. However, the assembly of albumin into water-insoluble materials at such a large scale seems to be a complex phenomenon relying on more than just the salting-out of the protein. For example, Na^+ and K^+ were considered to have similar lyotropic properties according to the Hoffmeister classification. However, when it came to albumin assembly into materials, NaBr and KBr led to opposite outcomes, where only NaBr led to the formation of water-insoluble materials.

The water solubility of the salt seems to be an important factor, as the group of salts inducing the formation of stable materials has the highest solubility. Furthermore, we showed that the following parameters "salt concentration" and "albumin concentration" are linked, as the molar ratio salt/albumin represented the best parameter to predict albumin materials formation (Figure S4, Supporting Information). The investigation of the pH on the formulation revealed that albumin assembled into water-insoluble membranes independently of pH within the tested pH range (from pH 4 to 8, Figure S5, Supporting Information).

Our results are surprising because salts such as NaBr are not known to induce protein crosslinking. Furthermore, at this stage, we can only hypothesize on how these materials form and we do not have a definite answer about the formation mechanism. The formation mechanism seems to be complex and probably involves multiple factors that we will have to investigate in the future and not the purpose of this paper. Our first aim here is to provide a full description of the material and to demonstrate its excellent biocompatibility for future applications.

BSA/NaBr membranes were selected to further characterize these materials. These materials were obtained by evaporating a solution of BSA (100 mg mL^{-1}) and NaBr (1 M) at pH 6 for 7 days at 37 °C (for each membrane: mass of BSA deposited in the mold ≈800 mg, surface of the mold ≈7 cm^2). After washing and drying at 37 °C for 24 h, the materials were produced with a relative yield (ratio between the dry mass of the washed material and the initial mass of albumin used in the formulation) higher than 80% and had a density of 1.29 ± 0.02 g cm^{-3} (determined using immersion method). Surface analysis (SEM, contact angle measurements) of BSA/NaBr membranes (details in the Supporting Information) revealed that they had a rough surface with low wettability (Figure S6, Supporting Information).

3.3. Salt-Compacted Albumin Materials are Stable in Aqueous Solutions and Biodegradable by Protease

The stability in aqueous solutions of BSA/NaBr membranes was determined by measuring their mass loss after incubation for 7 days at 37 °C in various media (water, physiological saline solution, 1 M NaCl solution, 1 M NaBr solution, and ethanol) (Figure 1C). The mass loss did not exceed 10% for all tested membranes except those incubated at pH 10, which lost 17% of their mass. Additionally, after incubation of the membranes in cell culture media (RPMI, RPMI with FBS 10% and MH, 7 days, 37 °C, under sterile conditions), they did not show any signs of degradation (less than 10% mass loss) (Figure S7, Supporting Information). When incubated in a solution of trypsin, an enzyme that is able to cut proteins, mainly at the carboxyl side of the amino acid lysine or arginine the membranes were entirely dissolved after 24 h, indicating their biodegradability by proteases. Moreover, BSA/NaBr membranes did not dissolve when incubated for 48 h in solutions of urea (8 M) and 2-mercaptoethanol (0.1 M), known to induce protein unfolding through hydrogen bond and disulfide bridge disruption.[37] This suggests that the self-assembly of the albumin into the material is not related to hydrogen bonding or the formation of disulfide bridges (Figure S8, Supporting Information). Therefore, the designed albumin membranes were stable in aqueous solutions and in cell culture media and biodegradable only by proteolytic enzymes.

3.4. Salt-Compacted Materials have Cartilage-Like Stiffness and Consist of a Network of Non-Denatured Albumin Nanoparticles Behaving Like a Physical-Chemical Gel

The mechanical properties of a biomaterial are a key factor in determining whether it is able to withstand biological environments [7] and is favorable to cellular proliferation and/or differentiation.[40,41] The stiffness of BSA/NaBr membranes hydrated in water was evaluated using tensile testing by applying a strain to the membranes with a constant rate until their rupture (Figures S9 and S10, Supporting Information). Young modulus, strain to rupture, and maximum stress of the membranes were determined by analyzing the stress–strain curves. Young modulus of the membranes was 0.86 ± 0.13 MPa (n = 5), lying in the range of the modulus of articular cartilage (0.3–0.9 MPa)[42,43] and higher than the modulus measured in albumin hydrogels and

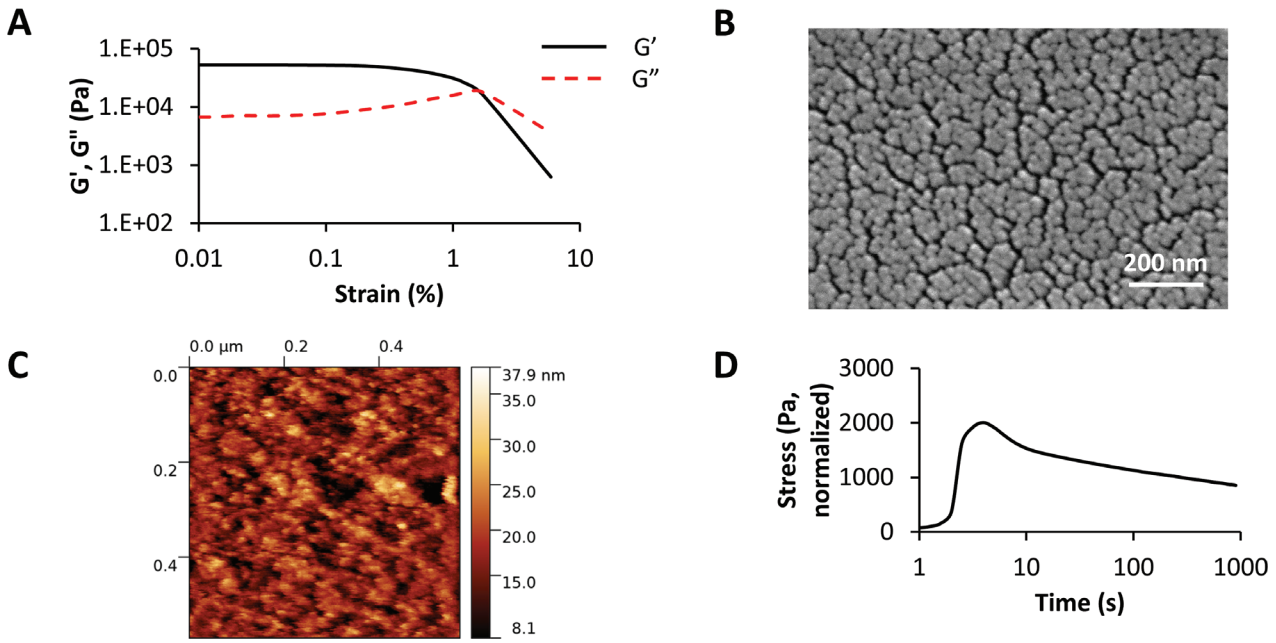

Figure 2. Rheological evaluation of the viscoelastic behavior of BSA/NaBr membranes (hydrated in water). A) Amplitude sweep tests (frequency = 0.5 Hz, strain = from 0.01 to 100%, 25 °C). Storage (G', red curve) and loss (G", blue curve) modulus are represented as a function of the strain. G" modulus reaches a maximum (Payne effect). B) SEM analysis of the cross-section of BSA/NaBr membranes. C) AFM observation of BSA/NaBr membrane in the liquid phase. D) Relaxation time assay performed by applying a shear strain of 1% (15 min, 25 °C). The increase in stress to a maximum of 2005 Pa is attributed to the rise in applied force during the first 4 s of the experiment to reach the strain of 1%.

cross-linked scaffolds (1–100 kPa).[13,15,16,44] The rupture of the membranes was observed at a tensile stress of 0.19 ± 0.03 MPa and a strain of 26.2 ± 4.7%. Compression testing on these membranes led to similar results with a Young modulus ranging from 0.6 to 2 MPa according to the type of salt used and its molar ratio. (Figure S11, Supporting Information).

An amplitude sweep performed on BSA/NaBr membranes (hydrated in water, n = 4) revealed that these membranes behaved like a viscoelastic material in the tested range of shear strain (strain: from 0.01% to 100%, frequency = 0.5 Hz, temperature = 25 °C). In the Linear Viscoelastic Region (LVR, from 0.01% to 1% shear strain), G' (elastic component of the shear modulus) was higher than G″ (viscous component), indicating that BSA/NaBr membranes exhibited a dominant elastic behavior (**Figure** 2A). A Payne effect was identified as G″ reaches a maximum at a strain of 1.79 ± 0.07% (Figure 2B). This effect is characteristic of materials made of two phases, a matrix in which harder particles are suspended causing greater energy dissipation at certain deformations.[45,46] This effect has been described primarily in rubber elastomers loaded with carbon black particles and is attributed to the changes induced by the deformation of the microstructure of the material.[45,46] Thus, BSA materials consist of a matrix containing hard albumin particles. These findings were confirmed both by SEM analysis of the section of a BSA/NaBr material, revealing a particulate structure (sizes of particles of ≈20 nm) forming these materials (Figure 2B), and by liquid-phase AFM images in MilliQ water, showing surface roughness with identical particulate structures of 21.3 ± 2.7 nm (Figure 2C).

To further characterize the viscoelastic properties of BSA/NaBr membranes, a relaxation test was performed. This test was performed by applying a constant strain of 1% to the membranes for 15 min at 25 °C using a rheometer in a parallel configuration. The resulting stress decay (reduction in force over time) was recorded (Figure 2D). Rt1/2 (the time at which the measured shear stress was reduced by half) was determined at 260 ± 11 s. The curve stress = f(time) (time was represented on a logarithmic scale) revealed two linear domains. The first linear domain lies between 4 and 8 s (fast relaxation phase, stress decayed from 2005 and 1627 Pa). The second linear domain lies between 8 and 896 s (slow relaxation phase, stress decayed from 1627 to 858 Pa) (Figure 2D). Theoretical Rt1 and Rt2 (the time at which the material is relaxed and the measured shear stress = 0) were 161 ± 58 s and > 10^5 s respectively, indicating the material has a fast relaxation phase followed by a slow relaxation phase (Figure S12, Supporting Information). The deformation of these materials was time-dependent, resulting from two molecular processes: the conformational change of the network and the migration of the solvent. These processes result in viscoelasticity and poroelasticity (caused by solvent flow through the material's pores), which commonly coexist as time-dependent behavior in gels.[49,50] In response to applied strain, the reorganization of the matrix relaxes the initial stress over time. Weak interactions lead to a short stress-relaxation time, and covalent interactions lead to long stress-relaxation time. Chemical-physical gels exhibit complex stress relaxation behavior due to the presence of both covalent and non-covalent crosslinks.[47,48] These conclusions were corroborated by the results of the frequency sweep and the temperature sweep assays (Figure S13, Supporting Information).

In addition, small and wide-angle X-ray scattering measurements (SAXS, WAXS) (Figure S14, Supporting Information),[51–61] as well as FTIR analysis (Figures S15

and S16, Supporting Information),[24,62–66] were used to get further insight into the structure of these materials. Details of the analysis are given in the supporting information. These assays showed in BSA/NaBr membranes an increase in the proportion of interprotein B-sheets. We hypothesize that the cohesion of our materials relies on these new interprotein interactions. We know that materials cannot be formulated without salt, and we know that salt is absent from materials after washing. We believe that salt acts as a catalyst, helping to structure materials by promoting the establishment of interprotein interactions. Once these are established, the salt can be washed away without destabilizing the material.

3.5. Human Albumin forms stable materials by salt-assisted compaction and the concept is extended to other water-soluble proteins

Formulation of membranes with other albumin proteins has also been tested. HSA, which has a very close structure to BSA, and OVA, which has a structure and a molecular weight quite different from the two other proteins,[12] produced also water-insoluble materials (HSA/NaBr and OVA/NaBr) (Figures S17 and S18, Supporting Information). In addition, the formation of water-insoluble membranes from other albumin proteins (recombinant albumin, serum albumin from rabbit, rat, and porcine) as well as γ-globulin was confirmed (Figure S19, Supporting Information). The main limitation of the use of salt-assisted compaction for the preparation of protein-based material is the water solubility of the protein. The process does not seem to apply to proteins that are not water-soluble because it requires the preparation and evaporation of a solution of protein and salt in an aqueous media. Furthermore, the low solubility of the protein will lead to a significant increase in the formulation time because of the increase in the solution volume required to obtain materials with a sufficient thickness to be handable (higher than 100 µm). Therefore, salt-assisted compaction allows the preparation of various protein membranes and proves to be promising for the formulation of stable materials from water-soluble proteins.

3.6. Salt-Compacted Albumin Materials do not Induce Cytotoxicity or Macrophage-Mediated Inflammation In Vitro

Biocompatibility is the main requirement for materials developed for biomedical applications. Here, we investigated the biocompatibility of salt-compacted albumin materials by evaluating their cytotoxicity in vitro. The cytotoxicity of BSA/NaBr membranes and their extracts was evaluated in vitro according to the ISO standard 10993–5.

First, we assessed extract cytotoxicity according to IS 13485-5 standard by incubating BALB/c 3T3 fibroblasts for 24 h with dilutions of BSA/NaBr membrane extracts (12.5%, 25%, 50%, and 100% $v_{extract}/v_{fresh\ culture\ media}$). The extracts were prepared by incubating BSA/NaBr membranes in culture media for 72 h at 37 °C. The metabolic activity of these cells was measured to assess their viability. The viability of the cells treated with each extract dilution was not statistically different from the viability of untreated cells (**Figure** 3A), indicating that BSA/NaBr membrane extracts did not contain cytotoxic leachable derivatives.

Then, BSA/NaBr membrane cytotoxicity was evaluated by incubating BALB/c 3T3 cells in direct contact with these membranes. The viability of the cells cultivated on the membranes was not statistically different from the viability of the cells cultivated on the plastic substrate (positive control) (Figure 3B). Microscopic observations revealed that the fibroblasts were proliferating on the surface of the membranes (Figure 3C). Furthermore, we showed that MDCK epithelial cells adhered and proliferated on the surface of BSA/NaBr membranes, forming a monolayer of contiguous cells (Figure 3D,E). In conclusion, albumin materials prepared by salt-assisted compaction biomaterials were not cytotoxic and favorable to cell adhesion, suggesting good biocompatibility.

Macrophage response to BSA/NaBr membranes was evaluated in vitro by seeding RAW 264.7 macrophages with these membranes for 48 h and measuring the inflammation mediators in the supernatant. LPS (lipopolysaccharide), a well-known endotoxin described as an inflammation inducer, was added to the LPS-treated groups. As expected, LPS activation induced a significant increase of the nitrite and TNF-α concentrations in the culture media of the LPS-treated control (T(LPS), without membranes) (Figure 3F,G). Nitrite and TNF-α production was similar between the non-treated group and the group of macrophages cultivated with BSA/NaBr membranes. Microscopic examination of the morphology of the macrophages revealed that they exhibit a round morphology when proliferating around the membranes and on their upper surface, confirming that BSA/NaBr membranes did not induce macrophage activation (Figure S20, Supporting Information). Underneath the material, some activated macrophages were spotted due to their elongated morphology (Figure S20, Supporting Information). Their activation was explained by the limited circulation of culture media in that area and was linked to the slight increase in TNF-α production observed in Figure 3G. Moreover, the presence of BSA/NaBr membranes decreased significantly nitrite concentration measured after macrophage activation by LPS ($p < 0.05$) (Figure 3F). Our hypothesis is that the nitric oxide produced as a result of cell activation reacted with the membrane to form a well-known compound, S-nitrosoalbumin.[67] Therefore, the tested albumin membranes do not induce macrophage-mediated inflammation in vitro and also showed a tendency to attenuate the intensity of pro-inflammatory signals.

3.7. Salt-Compacted Albumin Materials are Biocompatible and Biodegradable in Nude Mice Model

The aim of this in vivo investigation was to evaluate the biocompatibility and the biodegradability of albumin materials prepared by salt-assisted compaction and to investigate the inflammatory response induced by these materials. For these assays, we prepared cylindrical implants following the same procedure as for the membrane, using a specific cylindrical mold for the evaporation of the solutions. These materials were then washed in milliQ water, dried, and sterilized using electron beam irradiation at 25 kGy. Before implantation, the materials were rehydrated in a PBS buffer to be isotonic to the implantation site.

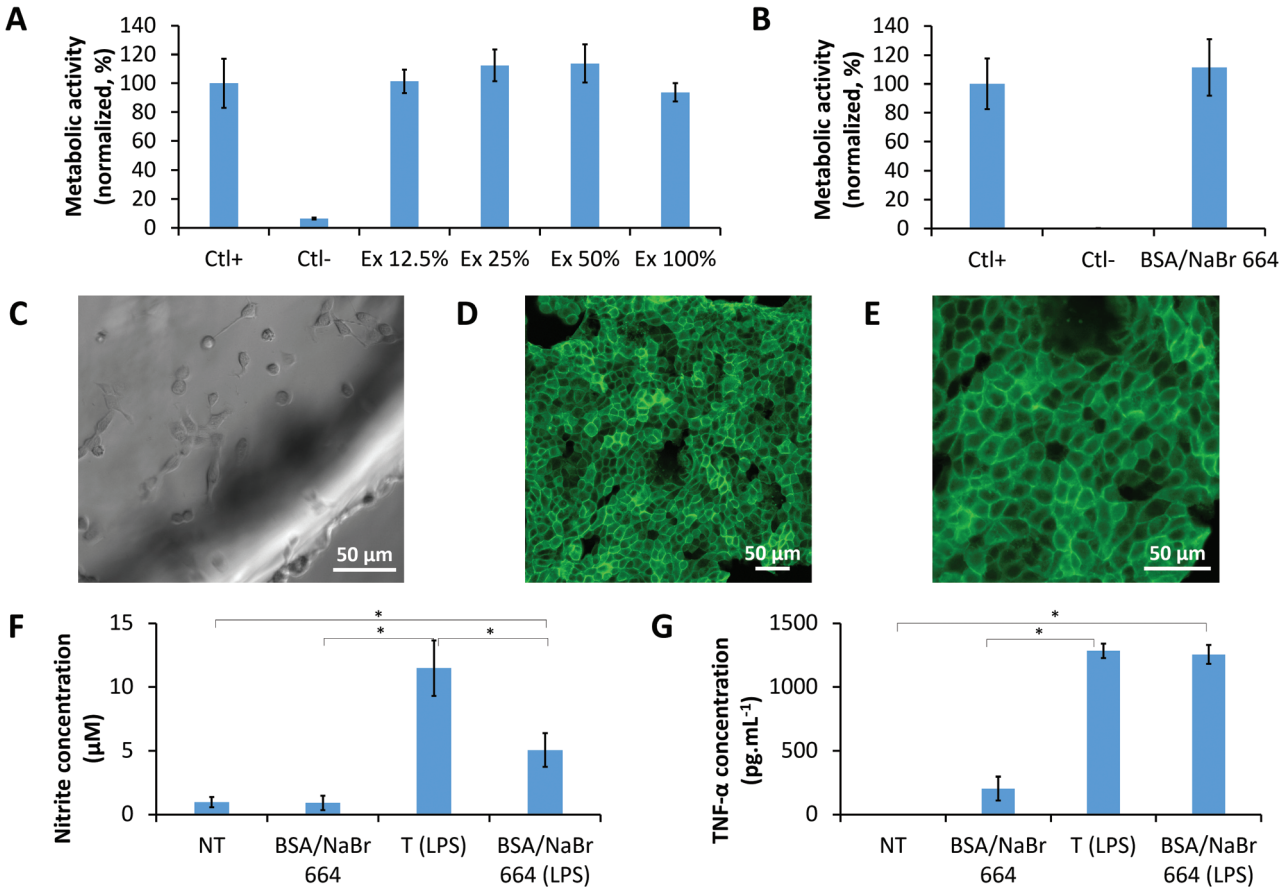

Figure 3. Biological evaluation in vitro of BSA/NaBr membranes (prepared with NaBr, molar ratio NaBr/albumin = 664). A) Viability (n = 4) of Balbc 3T3 cells cultivated for 24 h with dilutions (12.5%, 25%, 50%, and 100% v/v) of extracts prepared by incubating BSA/NaBr membranes in culture media (72 h, 37 °C). The cells of the positive (Ctl+) and negative (Ctl-) controls were incubated in culture media and 20% DMSO (diluted in culture media) respectively. B) Viability (n = 20) of Balbc 3T3 cells cultivated in direct contact with BSA/NaBr membranes. The controls, Ctl+ and Ctl-, were incubated in culture media and 20% DMSO (diluted in culture media) respectively. C) Balbc 3T3 cells on the surface of BSA/NaBr membranes. D,E) MDCK cells adhered on the surface of BSA/NaBr membranes and formed a monolayer of epithelial cells. F,G) Macrophage activation assessment (n = 8) by titration of nitrites and TNF-α in the supernatants after cultivation of RAW macrophages for 48 h with BSA/NaBr membranes. The non-treated group (NT) was cultivated without membranes and without LPS. LPS was added after 24 h (50 ng mL^{-1}) to all LPS-treated groups, including the LPS-treated control (T (LPS)). (*) A statistically significant difference was observed ($p < 0.05$).

NMRI-Nude mice were selected as the first in vivo model. This model is immunocompromised, therefore allowing the investigation of the degradation of the material by its surrounding tissues without the interference of the immune system. For this experiment, subcutaneous implantations of BSA/NaBr, BSA/$CaCl_2$, HSA/NaBr, and HSA/$CaCl_2$ cylindrical materials (**Figure 4A**) were performed in nude mice. Overall, all mice survived throughout the experiment and all implants were well tolerated with no clinical signs of toxicity, regardless of the type of albumin or salt used for the preparation of the materials. No statistically significant body weight difference was observed between the implanted groups during the month of experimentation (± 5% weight variation) (Figure 4C). After the sacrifice of the mice on day 28, histological evaluations showed that the tissues surrounding the implants were normal and that the formation and orientation of collagen fibers were similar to those observed in native tissue (Figure 4B). Therefore, albumin materials prepared by salt-assisted compaction did not lead to toxicity in mice, which demonstrates their in vivo biocompatibility.

The volumes of all implants decreased throughout the experiment, proving that these albumin materials were biodegradable in vivo probably through the activity of proteases. After 28 days, BSA/NaBr, BSA/$CaCl_2$, HSA/NaBr, and HSA/$CaCl_2$ implants lost respectively an average of 23%, 53%, 35%, and 43% of their initial volumes (Figure 4D). These results indicated that the enzymatic degradation of albumin materials in vivo was slow. Furthermore, the difference in degradation kinetics between formulations prepared with NaBr and $CaCl_2$ showed that the formulation parameters (salt type and concentration) can be tuned to control the degradation profile of albumin materials.

3.8. Salt-Compacted Albumin Materials do not Induce Systemic Toxicity and Inflammation in NZW Rabbits

Following the experimentations on Nude mice, the biocompatibility of albumin materials was tested on NZW rabbits. These animals were immunocompetent, therefore allowing the

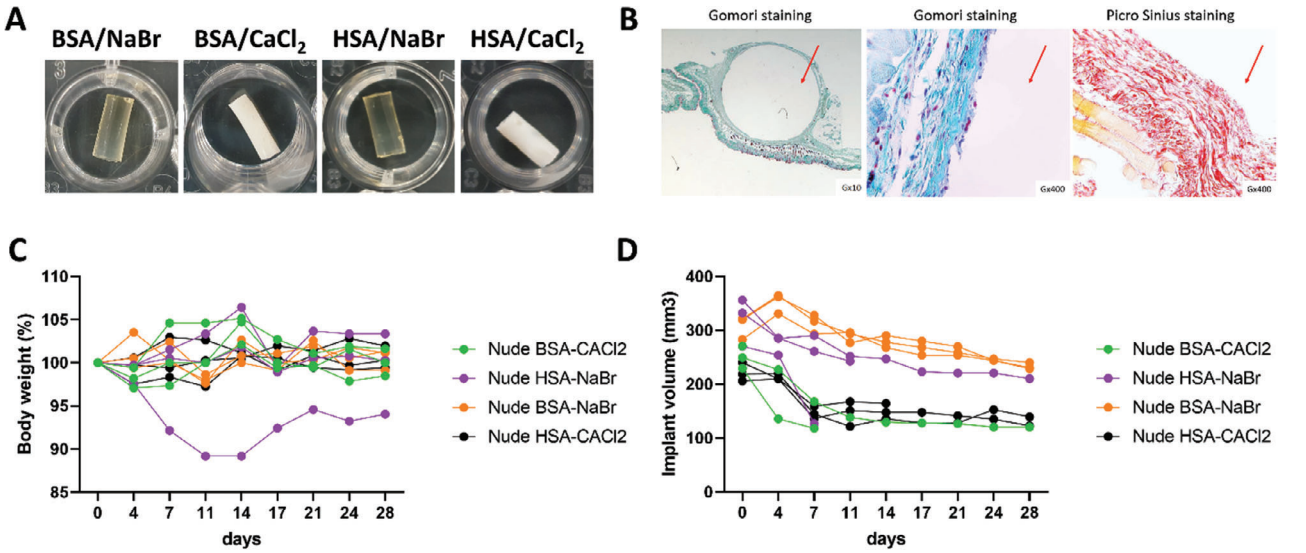

Figure 4. Biological evaluation of albumin materials implanted subcutaneously in NMRI-Nude mice for 28 days. A) Albumin cylindrical implants (≈5 mm in diameter and ≈10 mm in length). B) Histological evaluation of BSA/NaBr materials after mice sacrifice (the localizations of the implants are marked with red arrows). C) Body weight measurements of Nude mice implanted with albumin materials. D) Implant volume measurements during 28 days of subcutaneous implantation in Nude mice.

investigation of the inflammatory response to the implants throughout the experiments. Furthermore, the rabbit model allowed testing of implants prepared with autologous rabbit albumin (RbSA), in comparison to implants prepared with human albumin (HSA).

Subcutaneous implantation of RbSA/AcOK and HSA/$CaCl_2$ cylindrical materials was performed in the rabbits. An incision without implantation was performed on the control group. Overall, all rabbits survived during the study, and all implants were well tolerated with no clinical signs of toxicity, regardless of the type of albumin or salt used for the preparation of the materials. All animals of the three groups (control, RbSA/AcOK, and HSA/$CaCl_2$) showed a Draize score of 0 (absence of erythema and edema) throughout the study. Furthermore, no statistically significant difference in mean body weight was observed between the three groups at each time (**Figure** 5A).

Measurement of the sizes of the implants through the skin depicted an initial increase in their volume followed by a decrease in the second half of the experiment (Figure 5B). Between D2 and D13, the volumes of the RbSA/AcOK materials increased significantly up to 63.5% (1334 ± 308 mm^3 at D2) in comparison to D0 (815 ± 78 mm^3), then decreased from D16 to D27 up to 33.3% at D27 (544 ± 52 mm^3). As for the HSA/$CaCl_2$ materials, their volumes increased significantly up to 89.6% (917 ± 436 mm^3 at D2) compared to D0 (484 ± 83 mm^3) between D2 and D13, before regaining their initial values from D16 to D27. The observed increase in the volume of the materials can be related to the infiltration of subcutaneous fluids inside the implants.

The serum concentrations of ALAT and ASAT were measured to evaluate the systemic toxicity of the albumin materials. For RbSA/AcOK and HSA/$CaCl_2$ groups, the concentration of ALAT ranged between 41.60–56.27 IU and 26.67–39.60 IU respectively. As for ASAT serum concentration, it ranged between 15.37–52.37 IU and 16.20–21.70 IU for RbSA/AcOK and HSA/$CaCl_2$ groups respectively. No statistically significant difference in ALAT and ASAT serum concentrations was observed throughout the experiment between the implanted groups compared to the control group. Furthermore, for each group, no statistical difference was observed from D2 to D28 compared to D0. Therefore, albumin materials did not generate systemic toxicity after 28 days of implantation in rabbits (Figure 5C,D).

The evaluation of the systemic inflammation was performed by monitoring the concentration in the serum of various inflammation markers such as CRP, IL-6, IL-10, TNF-α, and IFN-γ throughout the experiment. Concerning CRP (**Table** 1) the normal values, determined with previous data collected by our subcontractor (C-Ris, France) and the literature, range from 3.4 to 80 µg mL^{-1}.[68,69] All CRP concentrations measured in our experiment were within this interval. A slight increase in CRP levels was observed in all groups at the beginning of the experiment. This variation was attributed to the surgical act and not to the implant since it decreased during the rest of the experiment. Furthermore, CRP levels were not statistically different between the implanted groups and the control group throughout the study.

Quantification of IL-6 showed that its serum concentration was below the LLOQ (12.5 pg mL^{-1}) for all rabbits (baseline level of IL-6 for male NZW rabbits ranging from 10 to 224.8

Table 1. Monitoring of the mean CRP concentration during the experiment.

	Mean CRP Concentration [µg mL^{-1}]		
Time (D)	Control	RbSA / AcOK	HSA / $CaCl_2$
0	3.36 (n = 1)*	8.51 (n = 2)*	3.86 (n = 2)*
2	26.54	29.81	13.11
14	8.58	16.67	4.22
28	41.90 (n = 2)*	< LLOQ	< LLOQ

* for the other individuals in the group the value was below the lower limit of quantification (LLOQ = 0,006 µg mL^{-1})

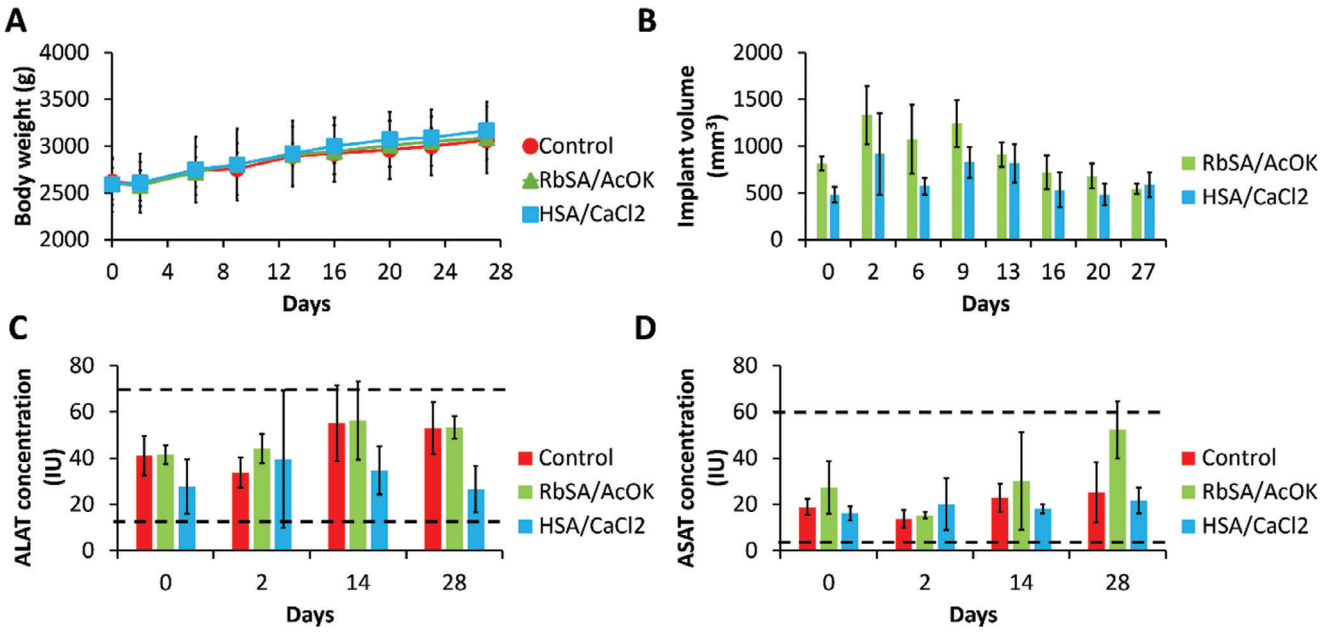

Figure 5. Biological evaluation of albumin materials implanted subcutaneously in NZW rabbits for 28 days. Surgical incision was performed on the control rabbits (n = 3) without implantation. Treated groups were implanted with HSA/$CaCl_2$ (n = 6) and RbSA/AcOK (n = 6) materials. A) Body weight measurements of NZW rabbits. B) Implant volume measurements. C-D) ALAT and ASAT titration in rabbit serum. The dashed line represents the range of concentrations commonly measured for rabbit controls (ALAT: 13–67 IU, ASAT: 3.8–60.4 IU).

pg mL^{-1}).[70–72] Similar results were obtained for IL-10, TNF-α and IFN-γ. The serum concentrations of these markers were below the LLOQ (78.1 pg mL^{-1}, 31.3 pg mL^{-1}, and 0.41 ng mL^{-1} respectively) and below the baseline levels for male NZW rabbits (under 50 pg mL^{-1}, between 25 and 91.20 and under 0.5 ng mL^{-1} respectively). Overall, the implantation of salt-compacted albumin materials did not induce an increase of inflammation markers, therefore, not inducing systemic inflammation after 28 days of implantation, regardless of the type of albumin used in the formulation. Furthermore, histopathologic examination of the implantation site showed minimal local inflammation and minimal fibrosis for both RbSA/AcOK and HSA/$CaCl_2$ groups. The HSA/$CaCl_2$ group displayed an overall higher local inflammation score than RbSA/AcOK implants. This observation was expected due to the autologous nature of RbSA for rabbits, unlike HSA. However, the high percentage of homology between these two proteins (≈75% identity) still allowed a good tolerance of HSA implants in rabbits.

4. Conclusion

In this study, we designed a new family of albumin materials using salt-assisted compaction, which is a very simple process based on the evaporation at 37 °C of a solution of albumin in the presence of salt. Through interactions with salts such as NaBr, NaI, KI, and $CaCl_2$, albumin is able to self-assemble into water-insoluble materials that are stable in different aqueous media while still biodegradable in the presence of proteases as demonstrated by in vivo experiments. The solubility of salts in water and their effect on the solubility of albumin seems to have a significant impact on the formation of this kind of material. The molar ratio between salt and albumin was identified as a key parameter in the formation of albumin membranes. In comparison with other formulation methods used to produce protein-based biomaterial, the method described in this study is relatively simple and allows for the one-step preparation of stable materials with good mechanical properties and Young's modulus comparable to that of cartilage without the need for any chemical crosslinking. The compaction of albumin through β structures and physical-chemical interactions demonstrates the material is water-insoluble and forms a stable material without crosslinking agents. Furthermore, it was shown that the same process allows for the preparation of autologous materials from human albumin, as well as other protein-based materials such as γ-globulin membranes. Albumin materials are biocompatible and biodegradable in vitro and in vivo they are non-inflammatory as they do not induce macrophage-mediated inflammation in vitro or systemic inflammation in vivo. These innovative materials constitute an outstanding new class of biomaterial with a wide range of applications, such as in tissue engineering scaffolds and in drug delivery devices. The production method is sufficiently versatile to produce a material whose shape, size, and various other properties are easily tunable to fit the requirements of targeted therapeutic applications. From a more fundamental point of view, the next steps will be devoted to better understanding the mechanisms involved in the interaction between salt ions and albumin leading to the formation of these new materials.

Supporting Information

Supporting Information is available from the Wiley Online Library or from the author.

Acknowledgements

The authors thank the Institute Carnot MICA (Propolpec project), SATT Conectus (Albupad project) and Agence Nationale de la Recherche (ANR-24-CE18-6089, "MEROU" project), for financial support. The project was also co-financed as part of the Offensive Science by the European Union's Interreg Upper Rhine program, the Grand Est Region, the Ministry of Science, Research and the Arts of Baden-Wurtemberg, the Minstry of Science and Health of Rhineland-Palatinate, the Canton of Basel Landschaft, the Canton of Basel-Stadt and the Swiss confederation.

Conflict of Interest

There are no conflicts to declare.

Data Availability Statement

The data that support the findings of this study are available from the corresponding author upon reasonable request.

Keywords

albumin, biodegradable materials, protein-based materials, salt-assisted compaction

Received: September 6, 2024
Revised: December 31, 2024
Published online:

[1] H. G. B. de Jong, H. R. Kruyt Koazervation, Z. Kolloid, **1930**, *50*, 39.
[2] G. Decher, M. Eckle, J. Schmitt, B. Struth, *Curr. Opin. Colloid. In.* **1998**, *3*, 32.
[3] C. H. Porcel, J. B. Schlenoff, *Biomacromolecules* **2009**, *10*, 2968.
[4] H. H. Hariri, J. B. Schlenoff, *Macromolecules.* **2010**, *43*, 8656.
[5] A. Reisch, P. Tirado, E. Roger, F. Boulmedais, D. Collin, J.-C. Voegel, B. Frisch, P. Schaaf, J. B. Schlenoff, *Adv. Funct. Mater.* **2013**, *23*, 673.
[6] R. R. Costa, A. M. S. Costa, S. G. Caridade, J. F. Mano, *Chem. Mater.* **2015**, *27*, 7490.
[7] M. N. Rodrigues, M. B. Oliveira, R. R. Costa, J. F. Mano, *Biomacromolecules* **2016**, *17*, 2178.
[8] T. Phoeung, M. V. Spanedda, E. Roger, B. Heurtault, S. Fournel, A. Reisch, A. Mutschler, F. Perrin-Schmitt, J. Hemmerlé, D. Collin, M. Rawiso, F. Boulmedais, P. Schaaf, P. Lavalle, B. Frisch, *Chem. Mater.* **2017**, *29*, 10418.
[9] A. Hardy, C. Seguin, A. Brion, P. Lavalle, P. Schaaf, S. Fournel, L. Bourel-Bonnet, B. Frisch, M. De Giorgi, *ACS Appl. Mater. Interfaces.* **2018**, *10*, 29347.
[10] R. Rohanizadeh, N. Kokabi, *J. Mater. Sci. -Mater. M.* **2009**, *20*, 2413.
[11] V. G. Arzumanyan, I. M. Ozhovan, O. A. Svitich, *Bull. Exp. Biol. Med.* **2019**, *167*, 763.
[12] T. Peters, *All About Albumin: Biochemistry, Genetics, and Medical Applications*, Academic Press, Cambridge, Massachusetts **1995**.
[13] J. Ong, J. Zhao, A. W. Justin, A. E. Markaki, *Biotechnol. Bioeng.* **2019**, *116*, 3457.
[14] H. T. Aiyelabegan, S. S. Z. Zaidi, S. Fanuel, A. Eatemadi, M. T. K. Ebadi, E. Sadroddiny, *Int. J. Polym. Mater. Po.* **2016**, *65*, 853.
[15] P.-S. Li, I.-L. Lee, W.-L. Yu, J.-S. Sun, W.-N. Jane, H.-H. Shen, *Sci. Rep.* **2015**, *4*, 5600.
[16] S. T. K. Raja, T. Thiruselvi, A. B. Mandal, A. Gnanamani, *Sci. Rep.* **2015**, *5*, 15977.
[17] G. Janarthanan, S. Lee, I. Noh, *Adv. Funct. Mater.* **2021**, *31*, 2104441.
[18] Y. Yamazoe (National Institue Of Advanced Industrial Science & Technology), JP20090216202 20090917, **2010**.
[19] H. Yamazoe, T. Tanabe, *J. Biomed. Mater. Res.* **2008**, *86A*, 228.
[20] L. Gallego, L. Junquera, Á. Meana, M. Álvarez-Viejo, M. Fresno, *J. Biomater. Appl.* **2010**, *25*, 367.
[21] D. Yoon, B.-J. Kang, Y. Kim, S. H. Lee, D. Rhew, W. H. Kim, O.-K. Kweon, *J. Vet. Sci.* **2015**, *16*, 397.
[22] N. Nseir, O. Regev, T. Kaully, J. Blumenthal, S. Levenberg, E. Zussman, *Tissue Eng. Part C-Me.* **2013**, *19*, 257.
[23] S. Fleischer, A. Shapira, O. Regev, N. Nseir, E. Zussman, T. Dvir, *Biotechnol. Bioeng.* **2014**, *111*, 1246.
[24] X. Zhou, Z. He, H. Huang, *Vib. Spectrosc.* **2017**, *92*, 273.
[25] A. Reisch, E. Roger, T. Phoeung, C. Antheaume, C. Orthlieb, F. Boulmedais, P. Lavalle, J. B. Schlenoff, B. Frisch, P. Schaaf, *Adv. Mater. Weinheim.* **2014**, *26*, 2547.
[26] P. Tirado, A. Reisch, E. Roger, F. Boulmedais, L. Jierry, P. Lavalle, J.-C. Voegel, P. Schaaf, J. B. Schlenoff, B. Frisch, *Adv. Funct. Mater.* **2013**, *23*, 4785.
[27] A. Mutschler, L. Tallet, M. Rabineau, C. Dollinger, M.-H. Metz-Boutigue, F. Schneider, B. Senger, N. E. Vrana, P. Schaaf, P. Lavalle, *Chem. Mater.* **2016**, *28*, 8700.
[28] L. Richert, P. Lavalle, E. Payan, X. Z. Shu, G. D. Prestwich, J.-F. Stoltz, P. Schaaf, J.-C. Voegel, C. Picart, *Langmuir* **2004**, *20*, 448.
[29] K. Kaibara, T. Okazaki, H. Bohidar, *Biomacromolecules* **2000**, *1*, 100.
[30] V. Boeris, B. Farruggia, G. Picó, *J Chromatogr B Analyt Technol Biomed Life Sci* **2010**, *878*, 1543.
[31] A. Michnik, K. Michalik, Z. Drzazga, *J. Therm. Anal. Calorim.* **2005**, *80*, 399.
[32] K. Baler, O. A. Martin, M. A. Carignano, G. A. Ameer, J. A. Vila, I. Szleifer, *J. Phys. Chem. B.* **2014**, *118*, 921.
[33] V. A. Borzova, K. A. Markossian, N. A. Chebotareva, S. Y.u. Kleymenov, N. B. Poliansky, K. O. Muranov, V. A. Stein-Margolina, V. V. Shubin, D. I. Markov, B. I. Kurganov, *PLoS One* **2016**, *11*, e0153495.
[34] M. G. Cacace, E. M. Landau, J. J. Ramsden, *Q. Rev. Biophys.* **1997**, *30*, 241.
[35] K. D. Collins, M. W. Washabaugh, *Q. Rev. Biophys.* **1985**, *18*, 323.
[36] P. Lo Nostro, B. W. Ninham, *Chem. Rev.* **2012**, *112*, 2286.
[37] Y. Zhang, P. S. Cremer, *Annu. Rev. Phys. Chem.* **2010**, *61*, 63.
[38] R. L. Baldwin, *Biophys. J.* **1996**, *71*, 2056.
[39] B. Kang, H. Tang, Z. Zhao, S. Song, H. Series, *ACS Omega.* **2020**, *5*, 6229.
[40] D. Huang, Y. Huang, Y. Xiao, X. Yang, H. Lin, G. Feng, X. Zhu, X. Zhang, *Acta Biomater.* **2019**, *97*, 74.
[41] M. d'Angelo, E. Benedetti, M. G. Tupone, M. Catanesi, V. Castelli, A. Antonosante, A. Cimini, *Cells* **2019**, *8*, 1036.
[42] R. K. Korhonen, M. S. Laasanen, J. Töyräs, J. Rieppo, J. Hirvonen, H. J. Helminen, J. S. Jurvelin, *J. Biomech.* **2002**, *35*, 903.
[43] L. E. Freed, R. Langer, I. Martin, N. R. Pellis, G. Vunjak-Novakovic, *Proc. Natl. Acad. Sci. USA.* **1997**, *94*, 13885.
[44] K. Baler, R. Michael, I. Szleifer, G. A. Ameer, *Biomacromolecules* **2014**, *15*, 3625.
[45] A. R. Payne, *J. Appl. Polym. Sci.* **1962**, *6*, 57.
[46] A. Lion, C. Kardelky, P. Haupt, *Rubber Chem. Technol.* **2003**, *76*, 533.
[47] X. Zhao, N. Huebsch, D. J. Mooney, Z. Suo, *J. Appl. Phys.* **2010**, *107*, 063509.
[48] Q.-M. Wang, A. C. Mohan, M. L. Oyen, X.-H. Zhao, *Acta Mech. Sin.* **2014**, *30*, 20.
[49] Y. Hu, Z. Suo, *Acta Mechanica Solida Sinica* **2012**, *25*, 441.
[50] W. Hong, X. Zhao, J. Zhou, Z. Suo, *J. Mech. Phys. Solids* **2008**, *56*, 1779.
[51] M. Hirai, H. Iwase, T. Hayakawa, K. Miura, K. Inoue, *J. Synchrotron Rad.* **2002**, *9*, 202.

[52] M. Hirai, S. Ajito, M. Sugiyama, H. Iwase, S. Takata, N. Shimizu, N. Igarashi, A. Martel, L. Porcar, *Physica B* **2018**, *551*, 212.
[53] B. Nagy, A. Tóth, I. Savina, S. Mikhalovsky, L. Mikhalovska, I. Grillo, E. Geissler, K. László, *Carbon* **2016**, *106*, 142.
[54] A. G. Kikhney, D. I. Svergun, *FEBS Lett.* **2015**, *589*, 2570.
[55] H. D. T. Mertens, D. I. Svergun, *J. Struct. Biol.* **2010**, *172*, 128.
[56] D. I. Svergun, M. H. J. Koch, *Rep. Prog. Phys.* **2003**, *66*, 1735.
[57] K. Yanase, R. Arai, T. Sato, *J. Mol. Liq.* **2014**, *200*, 59.
[58] L. Makowski, D. J. Rodi, S. Mandava, S. Devarapalli, R. F. Fischetti, *J. Mol. Biol.* **2008**, *383*, 731.
[59] L. Makowski, *J. Struct. Funct. Genomics.* **2010**, *11*, 9.
[60] D. Svergun, C. Barberato, M. H. J. Koch, *J. Appl. Crystallogr.* **1995**, *28*, 768.
[61] S. Bucciarelli, S. R. Midtgaard, M. Nors Pedersen, S. Skou, L. Arleth, B. Vestergaard, *J. Appl. Crystallogr.* **2018**, *51*, 1623.
[62] J. L. R. Arrondo, A. Muga, J. Castresana, F. M. Goñi, *Prog. Biophys. Mol. Bio.* **1993**, *59*, 23.
[63] J. C. Ioannou, A. M. Donald, R. H. Tromp, *Food Hydrocolloids.* **2015**, *46*, 216.
[64] A. Barth, *BBA-Bioenergetics* **2007**, *1767*, 1073.
[65] C. Guo, X. Guo, W. Chu, N. Jiang, H. Li, *Chinese Chem. Lett.* **2019**, *30*, 1302.
[66] G. Güler, M. M. Vorob'ev, V. Vogel, W. Mäntele, *Spectrochim. Acta A.* **2016**, *161*, 8.
[67] J. S. Stamler, O. Jaraki, J. Osborne, D. I. Simon, J. Keaney, J. Vita, D. Singel, C. R. Valeri, J. Loscalzo, *Proc. Natl. Acad. Sci. U.S.A.* **1992**, *89*, 7674.
[68] S. Pérez-Baos, P. Gratal, J. I. Barrasa, A. Lamuedra, O. Sánchez-Pernaute, G. Herrero-Beaumont, R. Largo, *Journal of Inflammation* **2019**, *16*, 2.
[69] R. D. Little, I. Prieto-Potin, S. Pérez-Baos, A. Villalvilla, P. Gratal, F. Cicuttini, R. Largo, G. Herrero-Beaumont, *Sci. Rep.* **2017**, *7*, 6311.
[70] R. Zhang, S. Chen, H. Zhang, Q. Liu, J. Xing, Q. Zhao, Y. Wang, B. Yu, J. Hou, *Sci. Rep.* **2016**, *6*, 33657.
[71] Y. Chen, Y. L. Traore, S. Yang, J. Lajoie, K. R. Fowke, D. W. Rickey, E. A. Ho, *J Control Release* **2018**, *277*, 102.
[72] S. R. Karthick, R. K. Sen, N. R. Gopinathan, M. S. Dhillon, R. Nada, R. R. Sharma, *J Clin Orthop Trauma* **2020**, *11*, S86.